Constraints on sterile neutrino models from strong gravitational lensing, Milky Way satellites, and Lyman - α forest

Ioana A. Zelko[1],* Tommaso Treu[1], Kevork N. Abazajian[2], Daniel Gilman[3], Andrew J. Benson[4], Simon Birrer[5,6], Anna M. Nierenberg[7], and Alexander Kusenko[1,8]

[1] Department of Physics and Astronomy, University of California-Los Angeles, 475 Portola Plaza, Los Angeles, CA 90095
[2] Department of Physics and Astronomy, University of California, Irvine, Irvine, CA 92697, USA
[3] Department of Astronomy and Astrophysics, University of Toronto, 50 St. George Street, Toronto, ON, M5S 3H4, Canada
[4] Observatories of the Carnegie Institution for Science, 813 Santa Barbara Street, Pasadena, CA 91101
[5] Kavli Institute for Particle Astrophysics and Cosmology and Department of Physics, Stanford University, Stanford, CA 94305, USA
[6] SLAC National Accelerator Laboratory, Menlo Park, CA, 94025
[7] University of California Merced, Department of Physics 5200 North Lake Rd. Merced, CA 9534 and
[8] Kavli IPMU (WPI), UTIAS, The University of Tokyo, Kashiwa, Chiba 277-8583, Japan

(Dated: May 23, 2022)

The nature of dark matter is one of the most important unsolved questions in science. Some dark matter candidates do not have sufficient nongravitational interactions to be probed in laboratory or accelerator experiments. It is thus important to develop astrophysical probes which can constrain or lead to a discovery of such candidates. We illustrate this using state-of-the-art measurements of strong gravitationally-lensed quasars to constrain four of the most popular sterile neutrino models, and also report the constraints for other independent methods that are comparable in procedure. First, we derive effective relations to describe the correspondence between the mass of a thermal relic warm dark matter particle and the mass of sterile neutrinos produced via Higgs decay and GUT-scale scenarios, in terms of large-scale structure and galaxy formation astrophysical effects. Second, we show that sterile neutrinos produced through the Higgs decay mechanism are allowed only for mass > 26 keV, and GUT-scale scenario > 5.3 keV. Third, we show that the single sterile neutrino model produced through active neutrino oscillations is allowed for mass > 92 keV, and the 3 sterile neutrino minimal standard model (νMSM) for mass > 16 keV. These are the most stringent experimental limits on these models.

I. INTRODUCTION

Multiple observations imply that the mass content of the universe is dominated by an unknown type of matter [1], which contributes ∼25% of the total energy. This matter is not made of ordinary atoms; it has no significant electromagnetic interaction, and it is thus called "dark matter" (DM). The nature of DM is one of the most important questions in modern science, with critical implications spanning from particle physics to astrophysics and cosmology.

Many theoretical DM models have been proposed. A number of dark matter candidates fall into the class of cold dark matter (CDM) [2], made of collisionless particles considered "cold" due to their small velocity dispersion relative to the speed of light. This is the most popular model and it is extremely successful on supergalactic scales but there are open challenges at subgalactic scales [3]. For example, CDM predicts more satellites than are observed around galaxies like the Milky Way (MW), subhalos hosting the largest MW satellites are either under-dense or too small, and CDM predicts "cuspy" dark matter density profiles in contrast to the flatter cores observed in dwarf galxies and clusters. It is still unclear whether these challenges can be solved by a better understanding of baryonic processes, or whether alternative dark matter models are needed [e.g. 4, and references therein].

Plenty of DM models have been proposed to eliminate these small-scale tensions between observations and CDM. DM particles which are generated with higher velocity dispersions erase fluctuations in the matter power spectrum at scales smaller than a characteristic 'free-streaming length', suppressing structures below this scale. So-called 'hot' dark matter candidates such as standard neutrinos are ruled out by observations, as the mean DM component. However, a broad range of "warm" DM (WDM) with smaller but non-negligible free streaming lengths are viable. One popular class of WDM models are sterile neutrinos (SNs).

Sterile neutrinos [5] are particles with right-handed chirality, no charge, and no color charge, and therefore do not interact with standard model particles except via mixing with neutrinos, or via some non-standard-model interactions. They were first introduced for the purpose of explaining the masses of active (left-handed) neutrinos, and can have masses in the range from eV to the Planck scale. In the early universe they can decouple from the plasma before electron-positron annihilation, when they are still relativistic.

* Corresponding author; The code and data for this project can be found at https://github.com/ioanazelko/sterile-neutrinos-constraints.git

Dodelson and Widrow [6] first established the sterile neutrino as a well-motivated WDM candidate. The model presented by Dodelson and Widrow [6] (hereafter the DW model) adds a single sterile neutrino to the Standard Model with a coupling to the active neutrinos. The DW mechanism produces particles through neutrino oscillations at temperatures below a few GeV, such that they behave like WDM. The number of sterile neutrinos is not subject to anomaly cancellation or other constraints, and more than one sterile neutrino is possible. In the seesaw theory of neutrino masses, one needs at least two right-handed states [7], but more right-handed states are allowed. It is an open question how many of these states have masses in the keV range, where they can serve as dark matter. The popular neutrino minimal standard model (νMSM) postulates three right-handed neutrinos with masses below the electroweak scale [8].

Production of sterile neutrinos in the early universe can proceed in different ways, and the mode of their production determines the clustering properties of dark matter [9–11]. A population of dark-matter sterile neutrinos can be produced due to their mixing with active neutrinos, which results in active to sterile neutrino conversions [6, 12]. This mechanism produces WDM. In the presence of a sizeable lepton asymmetry, the active to sterile neutrinos conversions select a lower-momentum part of the thermal distribution, leading to somewhat colder dark matter, as was pointed out by Shi and Fuller (SF) [13].

SNs could also be produced through mechanisms other than active neutrino oscillations, including "freeze-in" production from decays of the inflaton [14] or an SU(2)×U(1) singlet Higgs boson [9, 10, 15]. Most of the sterile neutrinos production from oscillations (DW or SF) takes place at temperature ~ 0.1 GeV. In contrast, Higgs boson decays can produce a population of sterile neutrinos at a temperature $\sim$100 GeV. Subsequent cooling and entropy production dilutes and redshifts this population, making the resulting DM colder than the WDM produced by DW or SF. This model, which produces particles in the 1-10 keV range, has been shown to produce the correct dark matter abundance, resulting in the so-called "keV Miracle Model" [11].

Another possible production mechanism for sterile neutrinos is the split seesaw mechanism [16, hereafter KTY], part of the production mechanism at the grand unified theory scale (GUT). The model predicts two large and one small Majorana masses due to a natural separation of scales. The large Majorana masses allow for thermal leptogenesis, while the keV mass produces a DM candidate. The model can be embedded into an SO(10) Grand Unified Theory, or some other theory containing a gauge $U(1)_{B-L}$ symmetry. The resulting DM is even colder than the one in the models described above, due to a more significant amount of dilution and redshifting of sterile neutrinos as the plasma cools from the GUT-scale production temperature.

The sterile neutrino models described above could explain the unidentified 3.5 keV X-ray line found in observations of galaxies and clusters [17, 18], even if they do not account for 100% of DM. Furthermore, keV sterile neutrinos can have a dramatic effect on supernova explosions, for example, explaining the pulsar kick velocities in excess of 1000 km/s which so far has evaded other explanations [19, 20].

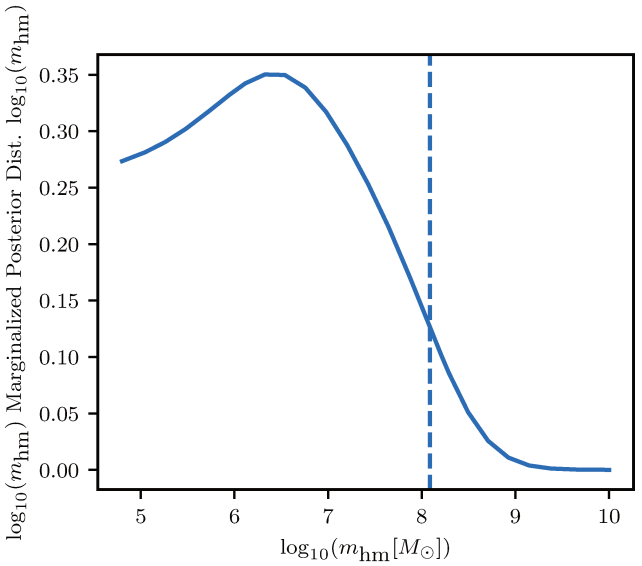

FIG. 1. Marginalized posterior for the $\log_{10}(m_{\rm hm})$, obtained by [21] from the analysis of eight quadruply imaged quasars.

We use state-of-the-art measurements of gravitationally lensed quasars, MW satellites, and Lyα, to constrain the 4 popular sterile neutrino models described above. We take their limits in terms of a traditional reference WDM model composed of a thermal relic, and compute the equivalent sterile neutrino models, from the point of view of cosmological structure formation and the halo mass function. As we will show, our analysis provides the most stringent limits to date on these four sterile neutrino models.

In § II we briefly review the strong gravitational lensing constraints on thermal relic WDM obtained by [21]. In § III, we derive a relationship between the masses of the thermal relic WDM particle and the astrophysically-equivalent sterile neutrinos dark matter particles. In § IV we use strong lensing, galaxy counts, and Lyman-α data to constrain the sterile neutrino models, eliminating part of the parameter space. We conclude in § V.

II. THERMAL RELIC WARM DARK MATTER CONSTRAINTS FROM STRONG GRAVITATIONAL LENSING

Strong gravitational lensing depends only upon gravity and is thus sensitive to the abundance of halos irrespective of their ability to emit or absorb light, making it a very powerful probe of the universe on subgalac-

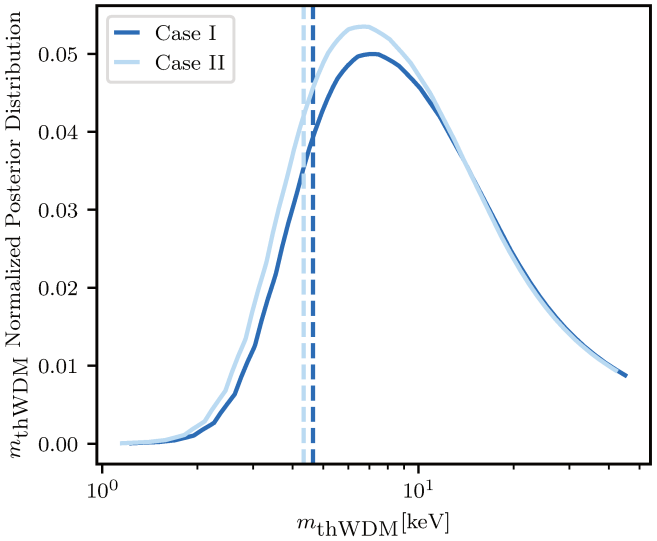

FIG. 2. Marginalized posterior of the masses of the thermal relic WDM particle. The vertical dotted line marks the 95% lower boundary interval, corresponding to 4.6 and 4.3keV, which represent the case where the assumption for the average background density of the universe includes (Case I), or does not include (Case II), baryonic matter in addition to dark matter (see Appendix).

tic scales. It can thus determine the halo mass function directly, avoiding uncertainties related to the physics of star formation in low mass galaxies that affect traditional methods based on counting photons.

[21] used eight quadruply-imaged quasars systems to constrain the amplitude of the halo mass function and the free-streaming length of dark matter. For each system, many realizations of dark matter structure are drawn from analytic dark matter halo mass functions flexible enough to describe mass functions produced by a broad range of thermal relic dark matter masses.

The predicted flux ratios for each realization are compared with the observed flux ratios to estimate the likelihood using Approximate Bayesian Computing. The likelihoods from each system are multiplied together to infer the parameters common to all systems. A key parameter is the 'half-model mass' $m_{\rm hm}$ which is the mass at which there are half as many halos as there would have been in the case of CDM.

We marginalize over all the other parameters to obtain the posterior distribution for $m_{\rm hm}$ shown in Fig. 1. As always in Bayesian statistics, the posterior depends on the choice of priors. Since we do not know the order of magnitude of the sterile neutrino mass we adopt a uniform prior in $\log 10(m_{\rm hm})$, within the range $10^{4.8} - 10^{10} M_\odot$.

The constraints on $m_{\rm hm}$ can be tied into constraints on the mass of the DM particle, given a model. A traditional reference model is the thermal relic WDM. It does not refer to a physical particle in particular, but serves as a standard tie-in model for the properties of WDM models with thermal relics. [22], [23] derived a one-to-one mapping between the half-mode mass and the mass of the thermal relic WDM. As detailed in the Appendix, the general form of the conversion is

$$m_{\rm thWDM} = 3.3 \left[\left(\frac{m_{\rm hm}[M_\odot]}{A} \right)^{-1/3.33} \right] \text{keV}, \quad (1)$$

$$p(m_{\rm thWDM}) = p(m_{\rm hm}) \frac{A}{3.3/3.33} \left(\frac{m_{\rm hm}[M_\odot]}{A} \right)^{4.33/3.33}, \quad (2)$$

where A has two possible values (Case I and II). Using Eq. 1 and 2, we obtain the posterior shown in Fig. 2.

III. RELATION BETWEEN THERMAL RELIC WDM AND STERILE NEUTRINO TRANSFER FUNCTIONS

Our goal is to use the constraints discussed as an illustration in §II, and those obtained by [24] and [25, 26] to constraints on the four sterile neutrino dark matter candidates discussed in §I: the GUT-scale scenario (KTY), the 'keV miracle model' Higgs production mechanism (PK), the single particle neutrino oscillation production mechanism (DW), and the Shi-Fuller mechanism within the neutrino minimal standard model (νMSM)..

The key quantity is the transfer function, T, which describes the effect of free-streaming on matter distribution. Given the power spectrum of initial density fluctuations P_i, T describes its evolution as a function of scale k and cosmic time, with respect to a standard CDM model:

$$T_s(k) \equiv \sqrt{\frac{P_{\rm sterile,i}(k)}{P_{\rm CDM,i}(k)}}, \quad (3)$$

The thermal relic WDM transfer functions for a given $m_{\rm thWDM}$ can be obtained from the analytical form presented in equation A9 of [22] (with more recent numbers from [27]), and it is given by

$$T_{\rm thWDM}(k) = \left[1 + (\alpha k)^{2\mu}\right]^{-5/\mu} \quad (4)$$

with α, μ given in the Appendix.

For the initial conditions, we fix the cosmology to the mean results from [1] and the CMB temperature from [28]: $H_0 = 67.36$, $\Omega_{\rm Matter} = 0.31530$, $\Omega_\Lambda = 0.68470$, $\Omega_{\rm Baryon} = 0.04930$, $\Omega_\nu = 0.00142$, $T_{\rm CMB} = 2.72548$K.

Remarkably, the transfer functions for thermal particles and sterile neutrinos are very similar, and one can approximate the other with a simple mapping of the relevant mass. This mapping allows one to convert any results obtained for thermal relic WDM to sterile neutrino in post-processing, without redoing the experiment or the analysis.

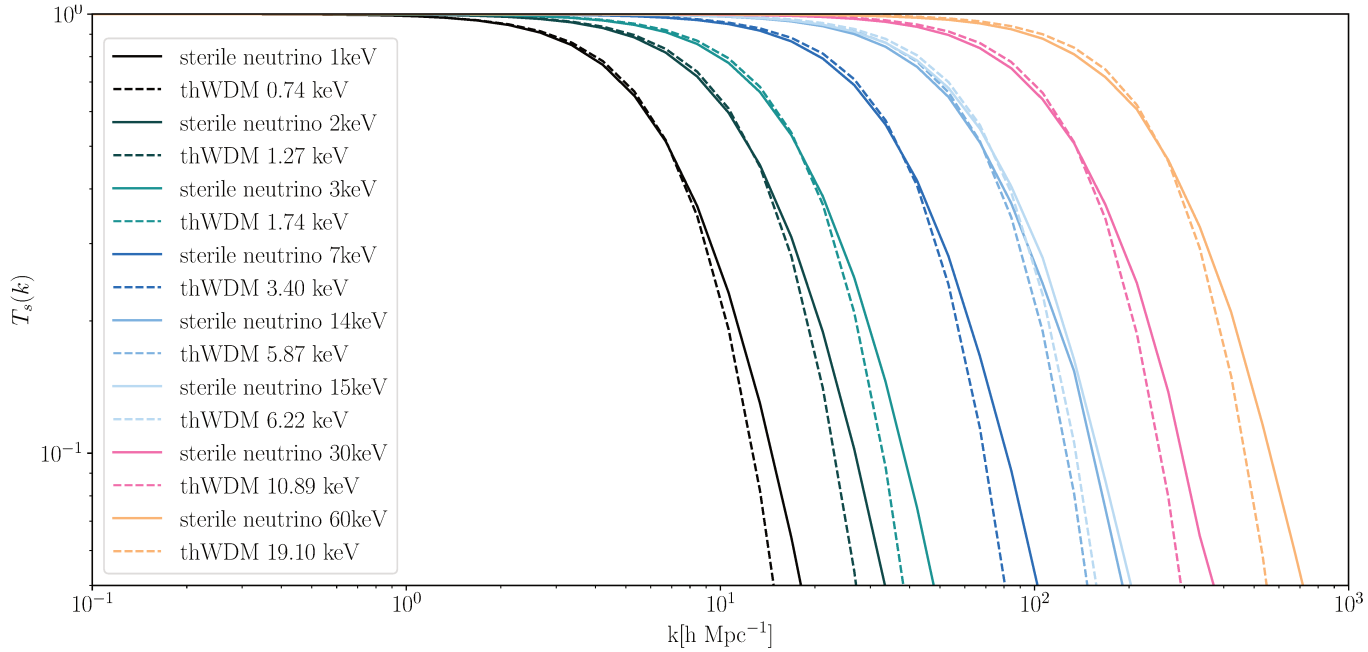

FIG. 3. Sterile neutrino transfer functions belonging to the Higgs decay (PK) model proposed by [10], shown by the continuous lines. The dotted lines show the corresponding thermal relic WDM transfer functions. As shown in [11], the two sets of functions are very similar to each other, thus allowing the possibility to create a mapping between the masses of thermal relic WDM particles and those of sterile neutrinos.

	deg	a_0	a_1	a_2
PK	1st	-3.26e+00	3.21e+00	
	2nd	-1.06e+00	2.31e+00	4.66e-02
KTY	1st	-1.10e+00	6.87e-01	
	2nd	-4.17e-01	5.11e-01	7.15e-03
power	law	a	b	
PK		1.56e+00	1.24e+00	
KTY		3.14e-01	1.24e+00	

TABLE I. Coefficients for the fits for the relation between the $m_{\rm sn}$ and $m_{\rm thWDM}$, for the cases of the Higgs production mechanism (PK) and GUT scale (KTY). The power law fit, as well as the first 2 degree polynomials are shown.

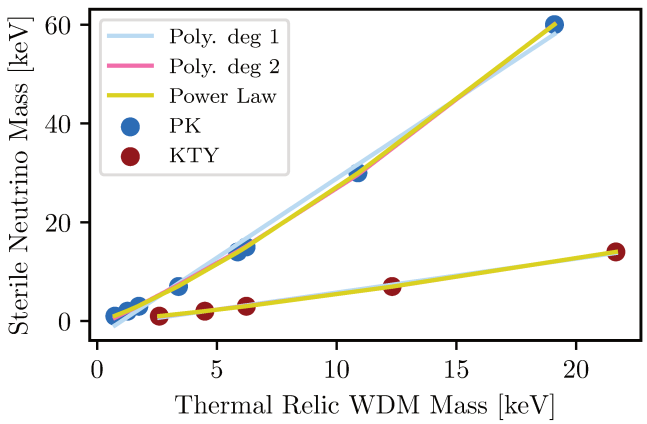

FIG. 4. The masses of the thermal relic WDM particles and sterile neutrino particles corresponding to the PK transfer functions shown in Fig. 3, as well as those for the KTY model, are shown as scattered points. Polynomial and power-law fits described by Eqs. 6 and 7 are shown as solid lines. These relations allow us to map constraints on the mass of thermal relic WDM to the corresponding mass of a sterile neutrino, for the 'kev miracle model' Higgs production mechanism (PK), and the GUT-scale scenario (KTY).

For sterile neutrinos produced through the oscillation mechanism for the Dodelson-Widrow model, the relation between $m_{\rm sn}$ and $m_{\rm thWDM}$ is taken from [27].

For the νMSM model, [29] derives the model connections to the half-mode mass $m_{\rm hm}$, and we use the posterior in Fig. 1 to constrain them.

Transfer functions for sterile neutrinos (Fig. 3) for the Higgs production mechanism and the GUT-scale scenarios have been previously obtained by [11]. The ones given here supersede the published ones by adopting more up to date cosmological parameters. We also corrected a mismatch between expected and provided dilution factors, using the non-CDM features of CLASS to calculate the transfer functions [30].

We tested two methods to find the relation between sterile neutrino and thermal relic WDM transfer functions: in the first, we fit the sterile neutrino transfer functions using the mass of the thermal relic WDM as a free parameter (Eq. 4); in the second, we match the 'half-mode' wavenumber where the transfer functions de-

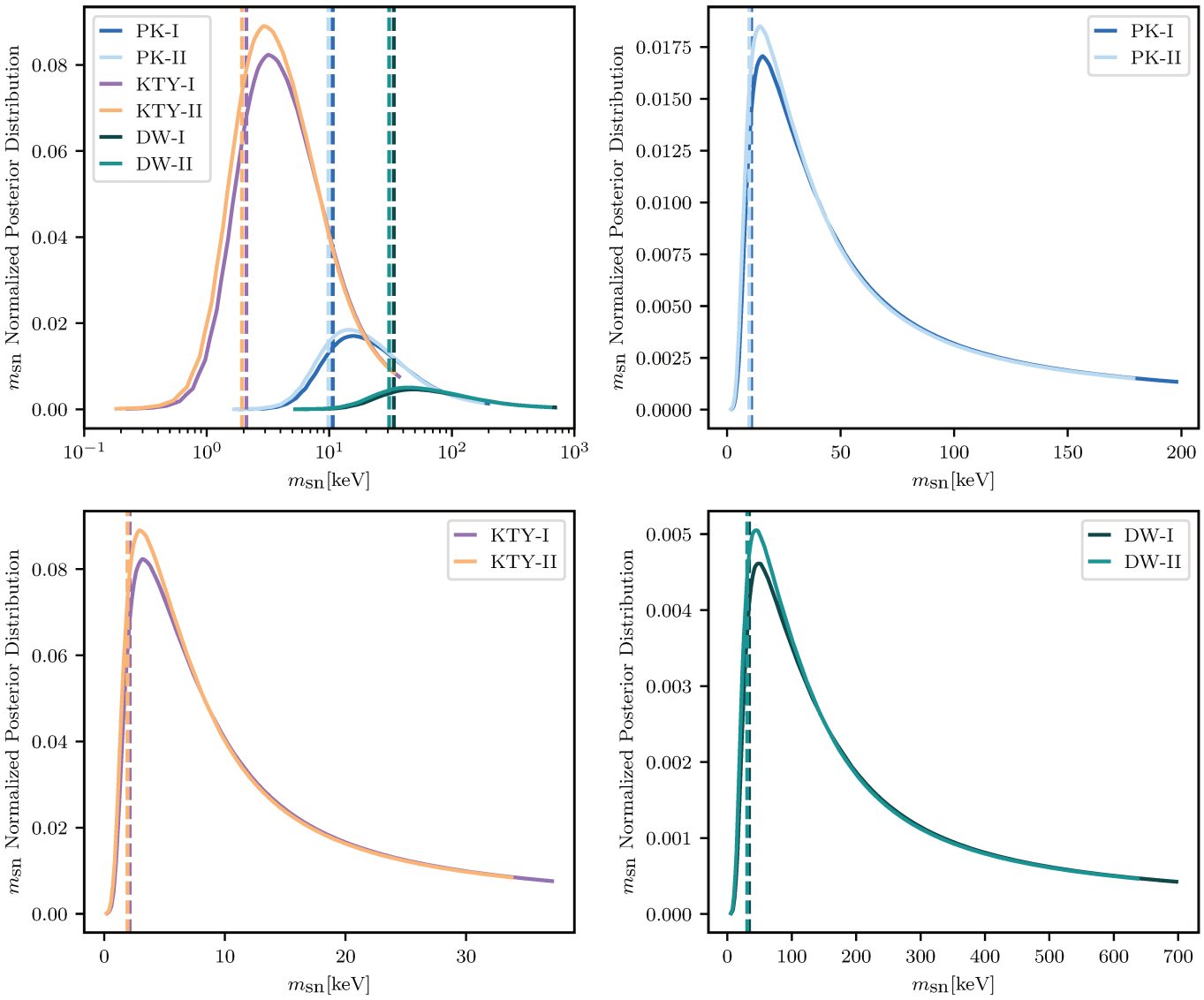

FIG. 5. Posterior probability distribution function $p(m_{\rm sn})$ of the mass of the various kinds of sterile neutrino: the GUT-scale scenario (KTY), the 'keV miracle model' Higgs production mechanism (PK), and single particle neutrino oscillation production mechanism (DW). The posteriors do not go to 0 on the right limit, so we cannot impose upper constraints on the particle masses; however, since they do go to 0 on the small limit, we can derive a lower limit. The vertical dotted line marks the 95% lower boundary interval, corresponding to 2.1/11/34 keV for KTY/PK/DW. The limits for the νMSM model depend on lepton asymmetry, and are discussed in the text.

crease to 0.5. For a given thermal relic WDM particle mass and transfer function, the half-mode $k_{\rm hm}$ and the mass of the particle $m_{\rm thWDM}$ can be related analytically from Eq. 4, to obtain:

$$m_{\rm thWDM} = k_{\rm hm}^{\frac{1}{1.11}} \left(0.049 \left(2^{\frac{\mu}{5}} - 1\right)^{-\frac{1}{2\mu}} \times \left(\frac{\Omega_X}{0.25}\right)^{0.11} \left(\frac{h}{0.7}\right)^{1.22}\right)^{\frac{1}{1.11}}. \quad (5)$$

In the first method, the fits might depend too much on how the numerical $T(k)$ for the sterile neutrinos was sampled, and the errors that arise at high k. The 1/2 mode matching gets rid of those issues, so we use this one for the rest of the paper. The difference in the end results of the two methods is of order 1%. We obtain the fits shown in Fig. 3.

The relation between the mass of the sterile neutrino which generates an equivalent transfer function to a thermal relic particle with a given mass can be approximated by a polynomial of degree *deg*:

$$m_{\rm sn} = f(m_{\rm thWDM}) = \sum_{0}^{deg} a_i \cdot m_{\rm thWDM}^i, \quad (6)$$

or by a power law:

$$m_{\rm sn} = a \cdot m_{\rm thWDM}^{b} \tag{7}$$

Results of the polynomials fits of orders 1, 2 (higher orders resulted in over fitting), as well as the power law, can be seen in Table I. Using these coefficients, a relation can also be derived between $m_{\rm sn}$ and $m_{\rm hm}$, seen below in the case of the power law fit:

$$m_{\rm sn} = a \cdot 3.3^{b} \left(\frac{m_{\rm hm}}{A}\right)^{-b/3.33} \tag{8}$$

where A takes the values described in the Appendix. These relations are calibrated on the $m_{\rm thWDM}$ mass interval of (0.75, 22) keV, and then extended to 60 keV when applied to data. Fig. 4 Shows the results of these fits. We use the results of the second order polynomial but we note that using a linear approximation would change the inferred bounds on sterile neutrino mass by only 11%.

IV. MAPPING THERMAL RELIC WARM DARK MATTER CONSTRAINTS ONTO STERILE NEUTRINOS

We obtain the most stringent experimental limits on four sterile neutrino models: PK, KTY, νMSM, and DW.

To recap, our starting point are the following 95% confidence limits on thermal relic WDM. The lensing-only analysis described in §II is $m_{\rm thWDM} > 4.6$keV [21]. Combination with satellite counts extends it to $m_{\rm thWDM} > 9.7\,$keV [24]. Independent work on the Lyman-α forest yields 3.3 keV [25] and 5.3 keV [26], the latter using additional assumptions for the relevant thermodynamics.

For the PK and KTY models, the relations derived in § III can now be used together with the ones for νMSM and DW to translate limits from thermal relic WDM into limits for the sterile neutrinos masses. The 95% limits for the four models are given in Tab. II.

We note that the posterior shown in Fig. 2 vanishes at the lower bound but not on the upper bound, as expected because the warmest models are ruled out by a number of observations. We thus convert the posteriors to lower limits, although of course the full posterior is more informative. Likelihood ratios can be obtained from Fig. 2.

For the νMSM model, we use the posterior on $m_{\rm hm}$ (Fig. 1) to eliminate the model space as shown in Fig. 2 of [29] , which presents the expected half-mode mass as a function of lepton asymmetry (L6) for different neutrino masses. Our upper limit on $\log_{10}(m_{\rm hm}[M_\odot])$from strong lensing alone is 8.1. This rules out masses under 7.0 keV for all lepton asymmetries. For higher masses, only limited ranges of lepton asymmetries are allowed: 7keV:L6 $\in$ (6.8, 7.6), 9keV: L6 $\in$ (5.2,7.8), 11keV:L6 $\in$ (4.3, 7.6), 14keV: L6 $\in$ (1.7, 7.9) , 16 keV: L6 $\in$ (1.6, 11.5). After incorporating the MW satellite counts constraints, $\log_{10}(m_{\rm hm}[M_\odot]) > 7.0$, which corresponds to $m_{\nu MSM} >$16keV. These limits offer an improved limits from existing work ([31]).

	Strong Lensing	Strong Lensing & Galaxy Counts	Lyman-α	Lyman-α & Thermo.
PK [keV]	I: 11 II: 9.8	I: 26 II: 24	7.1	12
KTY [keV]	I: 2.1 II: 1.9	I: 5.3 II: 4.9	1.3	2.5
νMSM [keV]	7.0	16	I: 5.0 II: 5.0	I: 9.0 II: 10
DW [keV]	I: 34 II: 31	I: 92 II: 84	21	40
$\log_{10}$ (hm[$M_\odot$])	8.1	7.0	I: 8.6 II: 8.5	I: 7.9 II: 7.8
thWDM [keV]	I: 4.6 II: 4.3	I: 9.8 II: 9.2	3.3	5.3

TABLE II. 95% lower limits for four sterile neutrino models: Higgs production mechanism (PK), GUT scale scenario (KTY), 3 sterile neutrino minimal standard model (νMSM), single model sterile neutrino produced through active neutrino oscillations (DW). The limits are derived from 4 datasets: gravitational strong lensing [21], strong lensing combined with Milky Way galaxy counts [24], Lyman-α forest [25], and Lyman-α forest combined with thermodynamic assumptions [26]. The case I and case II labels correspond to different assumption cases about the average background density of the universe, as described in the Appendix. In the last two raows of the table, we also presents the limits in terms of the half-mode mass, and the thermal relic WDM mass.

Future work would aim to combine the limits from strong lensing, galaxy counts, and Lyman-α forest in a joint analysis. Work has already been done in this direction ([32]), however their dataset obtained less stringent limits than the strong lensing combined with galaxy counts obtained by [24]. Future analysis combining the data sets used in Table II will be useful.

V. CONCLUSION

We used state-of-the-art measurements of strong gravitationally-lensed quasars, MW satellites, and Lyman-α forest to constrain four of the most popular sterile neutrino models.

First, we derive effective relations to describe the correspondence between the mass of a thermal relic WDM particle and the mass of sterile neutrinos produced via Higgs decay and GUT-scale scenarios, in terms of astrophysical effects. We take advantage of the similarity between the transfer functions of the sterile neutrinos mechanism presented by [11], and that of thermal relic WDM.

We note that our derived equivalence relation are of general importance, and can be used to put limits on

sterile neutrino models starting from any past or future thermal relic WDM measurement, not just the one we present here.

The limits on the PK, KTY, νMSM and DW models summarized in Table II are the most stringent experimental limits on these four models. We note that the limits from lensing and MW satellites are independent of and agree with those from the Lyα forest. We have effectively ruled out part of the parameter space for sterile neutrino generated through these 4 models.

ACKNOWLEDGMENTS

We acknowledge helpful conversations with Graciela Gelmini, Jiamin Hou, Doug Finkbeiner, Joshua Speagle, and Xiaolong Du

IZ and TT acknowledge support by the National Science Foundation grant NSF-1836016, by the Gordon and Betty Moore Foundation Grant 8548 and by NASA grant HST-GO-15177. Part of the data used in this paper were obtained as part of HST-GO-15177. SB is supported by the National Science Foundation through NSF AST-1716527. K.N.A. is supported in part by NSF Theoretical Physics Grant PHY-1915005. A.K. was supported by the U.S. Department of Energy (DOE) grant No. DE-SC0009937 and by Japan Society for the Promotion of Science (JSPS) KAKENHI grant No. JP20H05853, as well as by World Premier International Research Center Initiative (WPI), MEXT, Japan. This work was supported in part by the UC Southern California Hub, with funding from the UC National Laboratories division of the University of California Office of the President. This research made use of the NASA Astrophysics Data System's Bibliographic Services (ADS), the color blindness palette by Martin Krzywinski and Jonathan Corum[33], the Color Vision Deficiency PDF Viewer by Marie Chatfield [34], and the following software: CLASS [35], Jupyter Notebook [36], Mathematica [37], Matplotlib [38], NumPy [39], Python [40, 41], scikit-learn [42]

Appendix

The thermal relic WDM transfer functions can be approximated by an analytical function with a dependence on $m_{\rm thWDM}$, as show in equation A8 of [22], and Eq. 4. We use the more recent fit to the characteristic length scale factor $\alpha(m_{\rm thWDM})$ obtained by [27], with $\mu = 1.12$:

$$\begin{aligned}\alpha &= 0.049 \left(\frac{m_{\rm thWDM}}{\rm keV}\right)^{-1.11} \left(\frac{\Omega_{\rm thWDM}}{0.25}\right)^{0.11} \left(\frac{h}{0.7}\right)^{1.22} \\ &\equiv \lambda_{\rm fs}^{\rm eff}\end{aligned} \tag{A.1}$$

in units of Mpc h^{-1}. By convention, g is taken to be 1.5 for the warm particle, based on the equivalent contribution of a light neutrino species [22]. Following [23], we assume that the characteristic length scale α can be related to an effective free-streaming length scale $\lambda_{\rm fs}^{\rm eff}$.

The 'half-mode' length scale $\lambda_{\rm hm}$ corresponds to the scale at which the thermal relic WDM transfer function (4) decreases to 1/2:

$$\lambda_{\rm hm} = 2\pi\lambda_{\rm fs}^{\rm eff}(2^{\mu/5} - 1)^{-\frac{1}{2\mu}}. \tag{A.2}$$

We define the corresponding 'half-mode' mass scale and obtain a relation between $m_{\rm hm}$ and $m_{\rm thWDM}$:

$$\begin{aligned} m_{\rm hm} =& \frac{4\pi}{3}\bar{\rho}\left(\frac{\lambda_{\rm hm}}{2}\right)^3 = \frac{4\pi^4}{3}\bar{\rho}\left(2^{\mu/5}-1\right)^{-\frac{3}{2\mu}} {\lambda_{\rm fs}^{\rm eff}}^3 \\ =& \frac{4\pi^4}{3}\bar{\rho}\left(2^{\mu/5}-1\right)^{-\frac{3}{2\mu}} 0.049^3 \left(\frac{\Omega_{\rm thWDM}}{0.25}\right)^{0.33} \times \\ & \left(\frac{h}{0.7}\right)^{3.66} \left(\frac{m_{\rm thWDM}}{\rm keV}\right)^{-3.33} \\ =& A\left(\frac{m_{\rm thWDM}}{3.3{\rm keV}}\right)^{-3.33}, \end{aligned} \tag{A.3}$$

where $\bar{\rho}$ is the background density of the universe. The A constant thus depends on the assumed $\bar{\rho}$.

We consider two cases, where the background density of the universe can be taken as:

I. $\bar{\rho} = \Omega_{\rm M} \times \rho_{\rm critic}$, where $\Omega_{\rm M}$ includes the contributions of both baryonic and dark matter (as done in [24], or

II. $\bar{\rho} = \Omega_{\rm DM} \times \rho_{\rm critic}$, where only the contributions of dark matter are included (as done in [21]).

We thus obtain two equations between the 'half-mode' mass and the thermal relic mass:

$$\begin{aligned} &\text{I. } m_{\rm hm} = 3.81 \cdot 10^8 \left(\frac{m_{\rm thWDM}}{3.3{\rm keV}}\right)^{-3.33} M_\odot \\ &\text{II. } m_{\rm hm} = 3.04 \cdot 10^8 \left(\frac{m_{\rm thWDM}}{3.3{\rm keV}}\right)^{-3.33} M_\odot \end{aligned} \tag{A.4}$$

[1] P. Collaboration, Planck 2018 results. X. Constraints on inflation, Astronomy and Astrophysics **641**, A10 (2020).

[2] G. R. Blumenthal, S. M. Faber, J. R. Primack, and M. J. Rees, Formation of galaxies and large-scale structure with cold dark matter., Nature **311**, 517 (1984).

[3] J. S. Bullock and M. Boylan-Kolchin, Small-Scale Challenges to the ΛCDM Paradigm, Annual Review of Astronomy and Astrophysics **55**, 343 (2017).

[4] D. H. Weinberg, J. S. Bullock, F. Governato, R. Kuzio de Naray, and A. H. G. Peter, Cold dark matter: Controversies on small scales, Proceedings of the National Academy of Science **112**, 12249 (2015).

[5] A. Kusenko, Sterile neutrinos: The dark side of the light fermions, Physics Reports **481**, 1 (2009).

[6] S. Dodelson and L. M. Widrow, Sterile neutrinos as dark matter, Physical Review Letters **72**, 17 (1994).

[7] P. H. Frampton, S. L. Glashow, and T. Yanagida, Cosmological sign of neutrino CP violation, Phys. Lett. B **548**, 119 (2002), arXiv:hep-ph/0208157.

[8] T. Asaka and M. Shaposhnikov, The @nMSM, dark matter and baryon asymmetry of the universe [rapid communication], Physics Letters B **620**, 17 (2005).

[9] K. Petraki, Small-scale structure formation properties of chilled sterile neutrinos as dark matter, Phys. Rev. D **77**, 105004 (2008), arXiv:0801.3470 [hep-ph].

[10] K. Petraki and A. Kusenko, Dark-matter sterile neutrinos in models with a gauge singlet in the Higgs sector, Physical Review D **77**, 65014 (2008).

[11] K. N. Abazajian and A. Kusenko, Hidden treasures: Sterile neutrinos as dark matter with miraculous abundance, structure formation for different production mechanisms, and a solution to the σ₈ problem, Physical Review D **100**, 103513 (2019).

[12] K. Abazajian, Linear cosmological structure limits on warm dark matter, Physical Review D **73**, 63513 (2006).

[13] X. Shi and G. M. Fuller, New Dark Matter Candidate: Nonthermal Sterile Neutrinos, Physical Review Letters **82**, 2832 (1999).

[14] M. Shaposhnikov and I. Tkachev, The nuMSM, inflation, and dark matter, Phys. Lett. B **639**, 414 (2006), arXiv:hep-ph/0604236.

[15] A. Kusenko, Sterile neutrinos, dark matter, and the pulsar velocities in models with a Higgs singlet, Phys. Rev. Lett. **97**, 241301 (2006), arXiv:hep-ph/0609081.

[16] A. Kusenko, F. Takahashi, and T. T. Yanagida, Dark matter from split seesaw, Physics Letters B **693**, 144 (2010).

[17] E. Bulbul, M. Markevitch, A. Foster, R. K. Smith, M. Loewenstein, and S. W. Randall, Detection of An Unidentified Emission Line in the Stacked X-ray spectrum of Galaxy Clusters, Astrophys. J. **789**, 13 (2014), arXiv:1402.2301 [astro-ph.CO].

[18] A. Boyarsky, O. Ruchayskiy, D. Iakubovskyi, and J. Franse, Unidentified Line in X-Ray Spectra of the Andromeda Galaxy and Perseus Galaxy Cluster, Phys. Rev. Lett. **113**, 251301 (2014), arXiv:1402.4119 [astro-ph.CO].

[19] A. Kusenko and G. Segre, Neutral current induced neutrino oscillations in a supernova, Phys. Lett. B **396**, 197 (1997), arXiv:hep-ph/9701311.

[20] G. M. Fuller, A. Kusenko, I. Mocioiu, and S. Pascoli, Pulsar kicks from a dark-matter sterile neutrino, Phys. Rev. D **68**, 103002 (2003), arXiv:astro-ph/0307267.

[21] D. Gilman, S. Birrer, A. Nierenberg, T. Treu, X. Du, and A. Benson, Warm dark matter chills out: constraints on the halo mass function and the free-streaming length of dark matter with eight quadruple-image strong gravitational lenses, Monthly Notices of the Royal Astronomical Society **491**, 6077 (2020).

[22] P. Bode, J. P. Ostriker, and N. Turok, Halo Formation in Warm Dark Matter Models, The Astrophysical Journal **556**, 93 (2001).

[23] A. Schneider, R. E. Smith, A. V. Macciò, and B. Moore, Non-linear evolution of cosmological structures in warm dark matter models, Monthly Notices of the Royal Astronomical Society **424**, 684 (2012).

[24] E. O. Nadler, S. Birrer, D. Gilman, R. H. Wechsler, X. Du, A. Benson, A. M. Nierenberg, and T. Treu, Dark Matter Constraints from a Unified Analysis of Strong Gravitational Lenses and Milky Way Satellite Galaxies, The Astrophysical Journal **917**, 7 (2021).

[25] M. Viel, G. D. Becker, J. S. Bolton, and M. G. Haehnelt, Warm dark matter as a solution to the small scale crisis: New constraints from high redshift Lyman-α forest data, Physical Review D **88**, 43502 (2013).

[26] V. Iršič, M. Viel, M. G. Haehnelt, J. S. Bolton, S. Cristiani, G. D. Becker, V. D'Odorico, G. Cupani, T.-S. Kim, T. A. M. Berg, S. López, S. Ellison, L. Christensen, K. D. Denney, and G. Worseck, New constraints on the free-streaming of warm dark matter from intermediate and small scale Lyman-α forest data, Physical Review D **96**, 23522 (2017).

[27] M. Viel, J. Lesgourgues, M. G. Haehnelt, S. Matarrese, and A. Riotto, Constraining warm dark matter candidates including sterile neutrinos and light gravitinos with WMAP and the Lyman-α forest, Physical Review D **71**, 63534 (2005).

[28] D. J. Fixsen, The Temperature of the Cosmic Microwave Background, The Astrophysical Journal, Volume 707, Issue 2, pp. 916-920 (2009). **707**, 916 (2009).

[29] S. Vegetti, G. Despali, M. R. Lovell, and W. Enzi, Constraining sterile neutrino cosmologies with strong gravitational lensing observations at redshift z = 0.2, Monthly Notices of the Royal Astronomical Society **481**, 3661 (2018).

[30] D. Blas, J. Lesgourgues, and T. Tram, The Cosmic Linear Anisotropy Solving System (CLASS). Part II: Approximation schemes, Journal of Cosmology and Astroparticle Physics **2011**, 34.

[31] A. Dekker, S. Ando, C. A. Correa, and K. C. Y. Ng, Warm Dark Matter Constraints Using Milky-Way Satellite Observations and Subhalo Evolution Modeling (2021).

[32] W. Enzi, R. Murgia, O. Newton, S. Vegetti, C. Frenk, M. Viel, M. Cautun, C. D. Fassnacht, M. Auger, G. Despali, J. McKean, L. V. E. Koopmans, and M. Lovell, Joint constraints on thermal relic dark matter from strong gravitational lensing, the Ly α forest, and Milky Way satellites, Monthly Notices of the Royal Astronomical Society **506**, 5848 (2021).

[33] `http://mkweb.bcgsc.ca/biovis2012/color-blindness-palette.png`.

[34] `https://mariechatfield.com/simple-pdf-viewer/`.

[35] J. Lesgourgues, The Cosmic Linear Anisotropy Solving System (CLASS) I: Overview (2011).

[36] T. Kluyver, B. Ragan-Kelley, F. Pérez, B. Granger, M. Bussonnier, J. Frederic, K. Kelley, J. Hamrick, J. Grout, S. Corlay, P. Ivanov, D. Avila, S. Abdalla, and C. Willing, Jupyter Notebooks – a publishing format for reproducible computational workflows, in *Positioning and Power in Academic Publishing: Players, Agents and Agendas*, edited by F. Loizides and B. Schmidt (IOS Press, 2016) pp. 87–90.

[37] Wolfram Research Inc, Mathematica, {V}ersion 13.0.0 (2021).

[38] J. D. Hunter, Matplotlib: A 2D Graphics Environment, Computing in Science and Engineering **9**, 90 (2007).

[39] S. van der Walt, S. C. Colbert, and G. Varoquaux, The NumPy Array: A Structure for Efficient Numerical Computation, Computing in Science and Engineering **13**, 22 (2011).

[40] K. J. Millman and M. Aivazis, Python for Scientists and Engineers, Computing in Science and Engineering **13**, 9 (2011).

[41] T. E. Oliphant, Python for Scientific Computing, Computing in Science and Engineering **9**, 10 (2007).

[42] F. Pedregosa, G. Varoquaux, A. Gramfort, V. Michel, B. Thirion, O. Grisel, M. Blondel, A. Müller, J. Nothman, G. Louppe, P. Prettenhofer, R. Weiss, V. Dubourg, J. Vanderplas, A. Passos, D. Cournapeau, M. Brucher, M. Perrot, and É. Duchesnay, Scikit-learn: Machine Learning in Python (2012).

[43] P. Wizinowich, J. Chin, C. Correia, J. Lu, T. Brown, K. Casey, S. Cetre, J. R. Delorme, L. Gers, L. Hunter, S. Lilley, S. Ragland, A. Surendran, E. Wetherell, A. Ghez, T. Do, T. Jones, M. Liu, D. Mawet, C. Max, M. Morris, T. Treu, and S. Wright, Keck all sky precision adaptive optics, in *Society of Photo-Optical Instrumentation Engineers (SPIE) Conference Series*, Vol. 11448 (AA(W. M. Keck Observatory (United States)), AB(W. M. Keck Observatory (United States)), AC(W. M. Keck Observatory (United States)), AD(Univ. of California, Berkeley (United States)), AE(W. M. Keck Observatory (United States)), AF(W. M. Keck Observatory (U, 2020) p. 114480E.

[44] K. Abazajian, Production and evolution of perturbations of sterile neutrino dark matter, Physical Review D **73**, 63506 (2006).

[45] M. Oguri and P. J. Marshall, Gravitationally lensed quasars and supernovae in future wide-field optical imaging surveys, Monthly Notices of the Royal Astronomical Society **405**, 2579 (2010).

[46] T. Treu, A. Agnello, M. A. Baumer, S. Birrer, E. J. Buckley-Geer, F. Courbin, Y. J. Kim, H. Lin, P. J. Marshall, B. Nord, P. L. Schechter, P. R. Sivakumar, L. E. Abramson, T. Anguita, Y. Apostolovski, M. W. Auger, J. H. H. Chan, G. C. F. Chen, T. E. Collett, C. D. Fassnacht, J. W. Hsueh, C. Lemon, R. G. McMahon, V. Motta, F. Ostrovski, K. Rojas, C. E. Rusu, P. Williams, J. Frieman, G. Meylan, S. H. Suyu, T. M. C. Abbott, F. B. Abdalla, S. Allam, J. Annis, S. Avila, M. Banerji, D. Brooks, A. Carnero Rosell, M. Carrasco Kind, J. Carretero, F. J. Castander, C. B. D'Andrea, L. N. da Costa, J. De Vicente, P. Doel, T. F. Eifler, B. Flaugher, P. Fosalba, J. García-Bellido, D. A. Goldstein, D. Gruen, R. A. Gruendl, G. Gutierrez, W. G. Hartley, D. Hollowood, K. Honscheid, D. J. James, K. Kuehn, N. Kuropatkin, M. Lima, M. A. G. Maia, P. Martini, F. Menanteau, R. Miquel, A. A. Plazas, A. K. Romer, E. Sanchez, V. Scarpine, R. Schindler, M. Schubnell, I. Sevilla-Noarbe, M. Smith, R. C. Smith, M. Soares-Santos, F. Sobreira, E. Suchyta, M. E. C. Swanson, G. Tarle, D. Thomas, D. L. Tucker, and A. R. Walker, The STRong lensing Insights into the Dark Energy Survey (STRIDES) 2016 follow-up campaign - I. Overview and classification of candidates selected by two techniques, Monthly Notices of the Royal Astronomical Society **481**, 1041 (2018).

[47] A. M. Nierenberg, D. Gilman, T. Treu, G. Brammer, S. Birrer, L. Moustakas, A. Agnello, T. Anguita, C. D. Fassnacht, V. Motta, A. H. G. Peter, and D. Sluse, Double dark matter vision: twice the number of compact-source lenses with narrow-line lensing and the WFC3 grism, Monthly Notices of the Royal Astronomical Society **492**, 5314 (2020).

[48] A. M. Nierenberg, T. Treu, G. Brammer, A. H. G. Peter, C. D. Fassnacht, C. R. Keeton, C. S. Kochanek, K. B. Schmidt, D. Sluse, and S. A. Wright, Probing dark matter substructure in the gravitational lens HE 0435-1223 with the WFC3 grism, Monthly Notices of the Royal Astronomical Society **471**, 2224 (2017).

[49] A. M. Nierenberg, T. Treu, N. Menci, Y. Lu, P. Torrey, and M. Vogelsberger, The missing satellite problem in 3D, Monthly Notices of the Royal Astronomical Society **462**, 4473 (2016).

[50] A. M. Nierenberg, T. Treu, S. A. Wright, C. D. Fassnacht, and M. W. Auger, Detection of substructure with adaptive optics integral field spectroscopy of the gravitational lens B1422+231, Monthly Notices of the Royal Astronomical Society **442**, 2434 (2014).

[51] A. M. Nierenberg, T. Treu, N. Menci, Y. Lu, and W. Wang, The Cosmic Evolution of Faint Satellite Galaxies as a Test of Galaxy Formation and the Nature of Dark Matter, The Astrophysical Journal **772**, 146 (2013).

[52] A. M. Nierenberg, M. W. Auger, T. Treu, P. J. Marshall, C. D. Fassnacht, and M. T. Busha, Luminous Satellites. II. Spatial Distribution, Luminosity Function, and Cosmic Evolution, The Astrophysical Journal **752**, 99 (2012).

[53] A. M. Nierenberg, M. W. Auger, T. Treu, P. J. Marshall, and C. D. Fassnacht, Luminous Satellites of Early-type Galaxies. I. Spatial Distribution, The Astrophysical Journal **731**, 44 (2011).